Chapter 10

Small and large scale solar features

10.1 Coronal holes

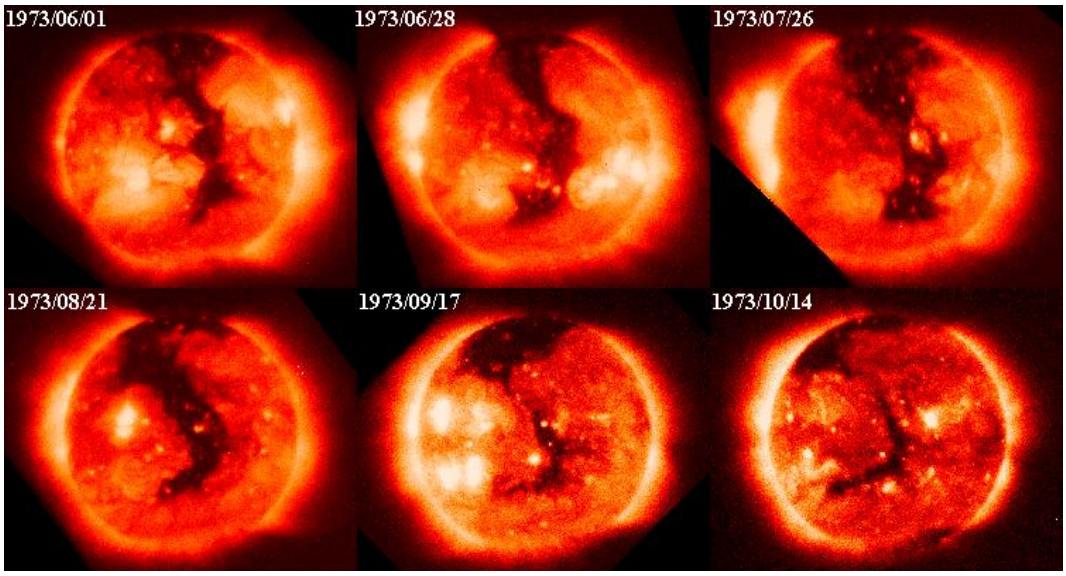

Figure 10.1: Skylab observations of a "boot of Italy" coronal hole. It survived over 4 months in 1973.

Definition of a coronal hole

- Brighter than the average solar surface at He I (10830 Å)
- Low contrast in cell structures
- Unipolar magnetic field
- High contrast at hole edges

+ particle density 2-3 times lower than in "quiet sun" regions.

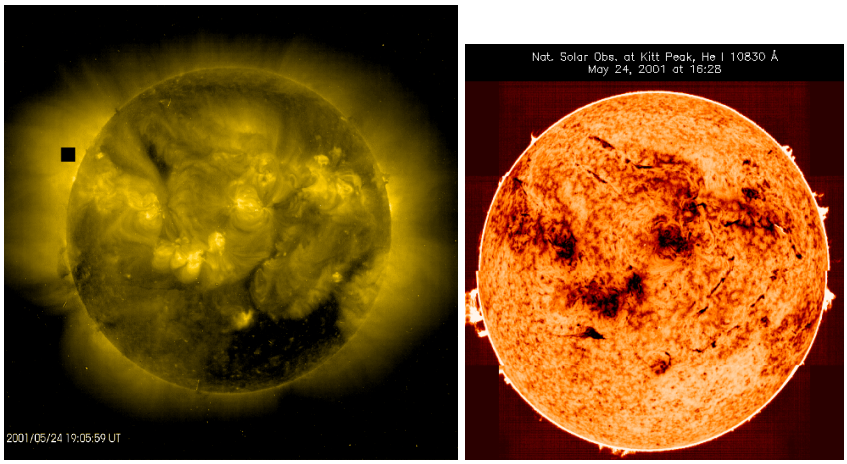

Figure 10.2: Left: EIT 284 Å (coronal hole visible as dark region). Right: Kitt Peak He I at 10830 Å (CH observed as bright).

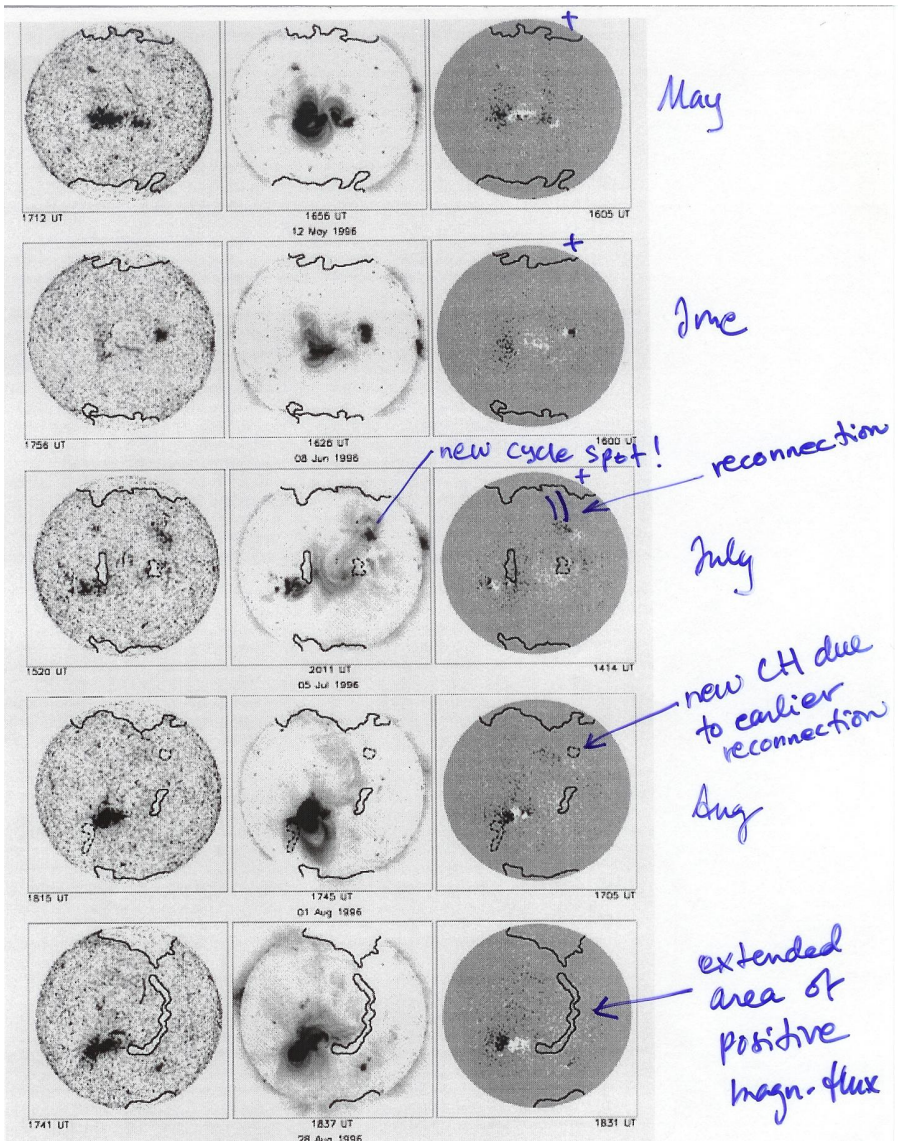

Figure 10.3: Harvey & Hudson (1998) explain CHs through emerging flux and reconnection. In this example, a new active region at ~N25 and the positive polarity polar region get connected and 'open' a new small coronal hole.

10.2 Radio-bright coronal holes

Polar radio brightenings:

- Discovered in the 1970s with the Crimean Astrophysical Observatory 22-m radio telescope
- Polar regions were observed to be brighter than the quiet Sun at 15–48 GHz (at <15 GHz they were depressed)
- At 22 GHz enhancement is about 1500 K, at 37 GHz 800 K (observed with 1-2 arc min spatial resolution)
- later Nobeyama high-resolution radio images showed diffuse brightenings near the poles but also compact bright separate sources

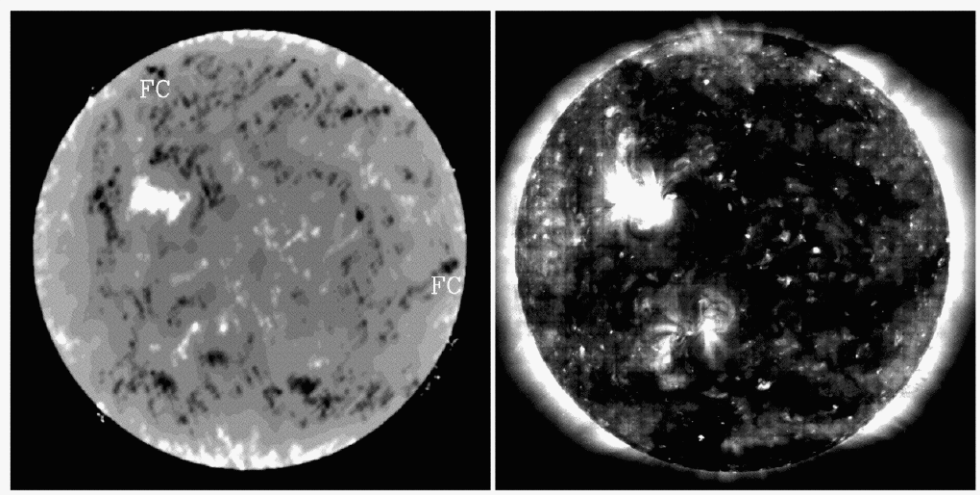

Figure 10.4: Polar radio brightenings: Nobeyama 17 GHz and EIT 195 Å observations of the Sun on 1997 March 11. The gray-scale range is chosen to emphasize the structure at the poles: in the 17 GHz image it ranges from 8000 K to 12,500 K in brightness temperature (Nindos et al., ApJ 527, 415-, 1999)

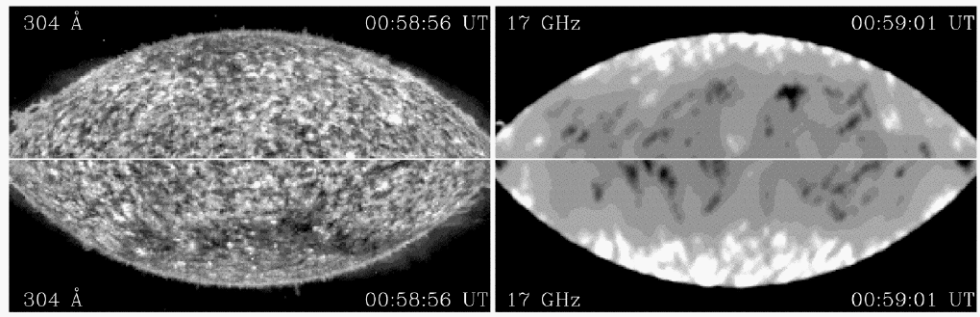

Figure 10.5: Polar radio brightenings: EIT images taken in the chromospheric line of He II at 304 Å on 1997 March 19 and the corresponding NRH 17 GHz maps. Top: north pole; bottom: south pole. The south pole 17 GHz emission is clearly more prominent (Nindos et al., ApJ 527, 415-, 1999)

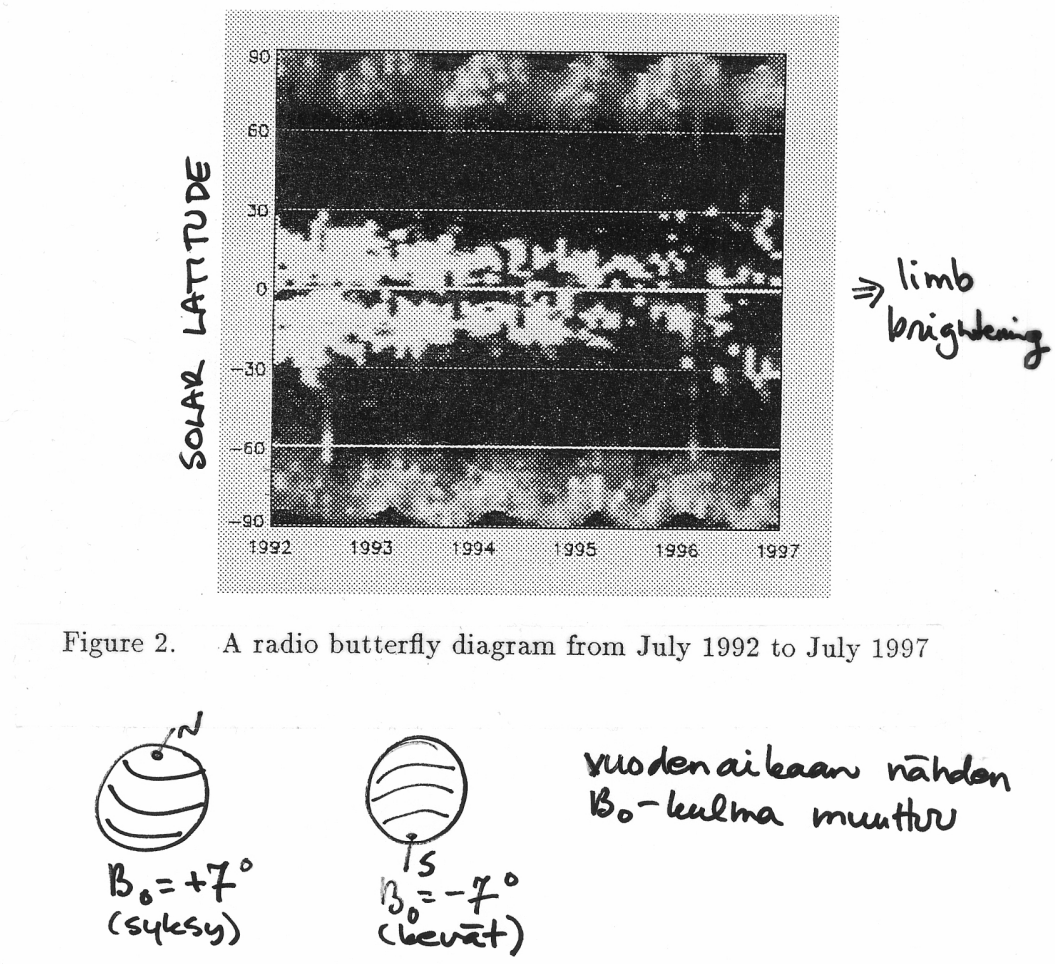

Figure 2. A radio butterfly diagram from July 1992 to July 1997

Equatorial coronal hole brightenings (radioheliograph observations at 17 GHz):

- CHs are basically unipolar magnetic field regions
- Diffuse brightenings (+500 K) inside network cells
- Compact brightenings (+2000 K) at network cell boundaries
- Temporal changes

Problems in measuring radio bright regions:

- Interferometers: how to deconvolve faint sources
- Single dish telescopes: not enough spatial resolution + instrumental limb darkening
- Magnetograms: difficult to measure field strengths near poles
- EUV and optical: difficult to define plasma volume

Candidates for the radio enhancements: bright points, bases of plumes, coronal hole edges, network structures, etc.

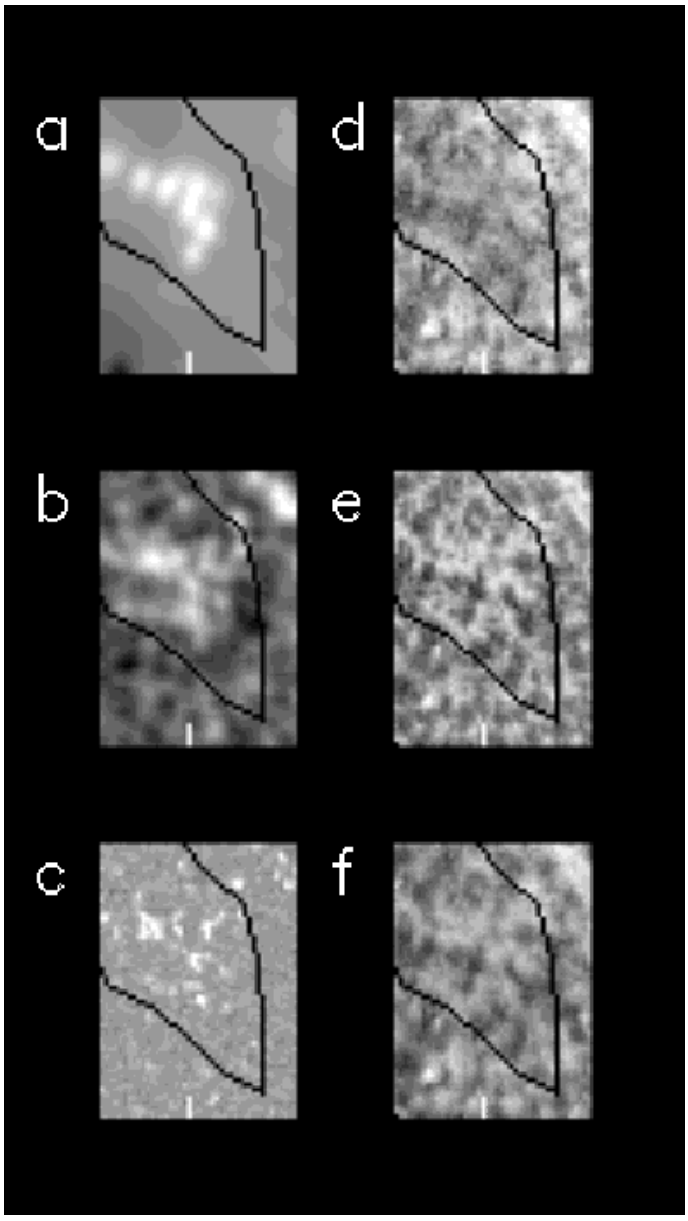

Figure 10.6: SUMER field of view subframes of the October 24, 1999 observations of an equatorial coronal hole (outlined with a black line). a) 17 GHz radio data, b) re-binned, smoothed Hα image, c) magnetogram, and SUMER d) O I 948.7 Å, e) HI Ly4 949.7 Å, and f) He II 958.6 Å images. Radio brightenings seem to correspond best to Hα structures (Moran et al., 2001).

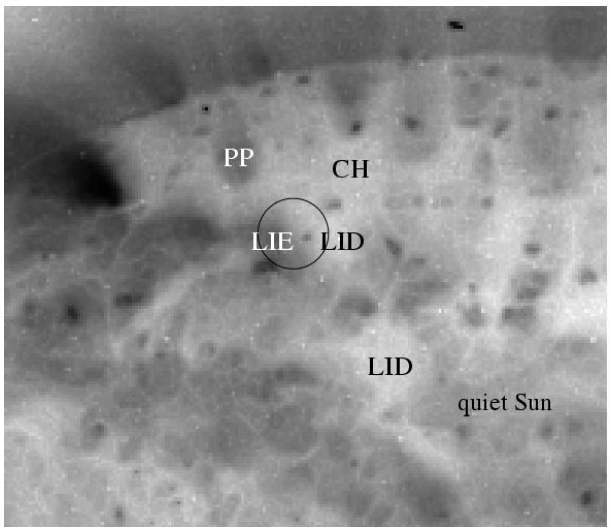

Figure 10.7: EIT map with radio beam size (circle), local intensity enhancement in EUV ('LIE') and local intensity decrease in EUV ('LID'). PP = polar plume and CH = coronal hole. It is evident that the radio flux within the beam is a convolution of several emission sources (Pohjolainen et al. 2000).

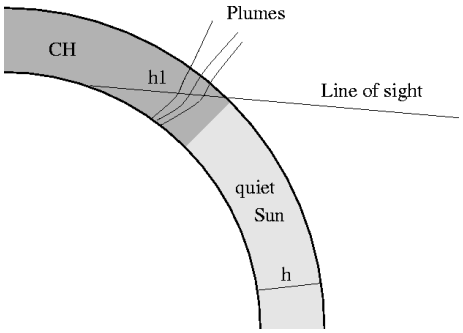

Figure 10.8: Geometry for observing the solar atmosphere at high latitudes: Polar coronal hole (CH) and the quiet Sun have scale height h and source length (radio path) L = near the poles. If the same atmospheric layer is viewed near the center of the disk, the source length L = h. Note that L for polar plumes is not significant unless the plumes are seen along the line of sight (from the top).

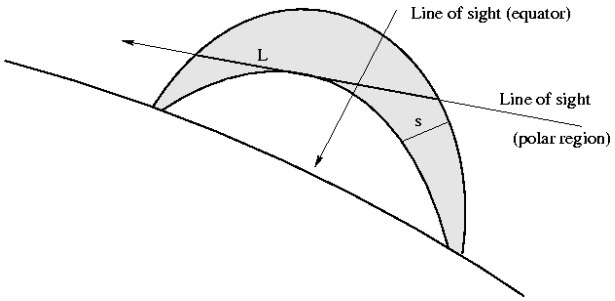

Figure 10.9: Observations of high latitude bright points with source length (radio path) L. If the loop (or a system of loops between two regions of opposite polarities) is viewed from the top (e.g., near the solar disk center), the source length L is equal to the loop diameter s.

10.3 Bright points

- Bipolar magnetic structures, size 10–50 arcsec
- Lifetime ~ 8 hours
- T ~ 2 MK, density ~ 2×10^9 cm^{-3}
- Hot plasma in small-scale loops
- Flaring bright point ⇒ cancelling flux / rising flux / rotational shear (convective motion) or ...?
- Images needed with better spatial resolution

Example: Brightness temperature of a bright point

$T_b = T_{eff}\ (1 - e^{-\tau})$

when $\tau \ll 1$, $T_b = T_{eff}\tau_\nu$

where $\tau_\nu = \kappa\, L \approx 0.01\ L\ \frac{n_e^2}{\nu^2 T^{3/2}} \times (24.5 + \ln T - \ln \nu)$

For a bright point,
s = 3500 km and L = 10 000 km
$T = 2 \times 10^6$ K
$n_e = 1.5 \times 10^9$ cm^{-3}
and at ν = 87 GHz, the temperature enhancement on top of the quiet Sun emission would be
⇒ $T_b \sim +30$ K

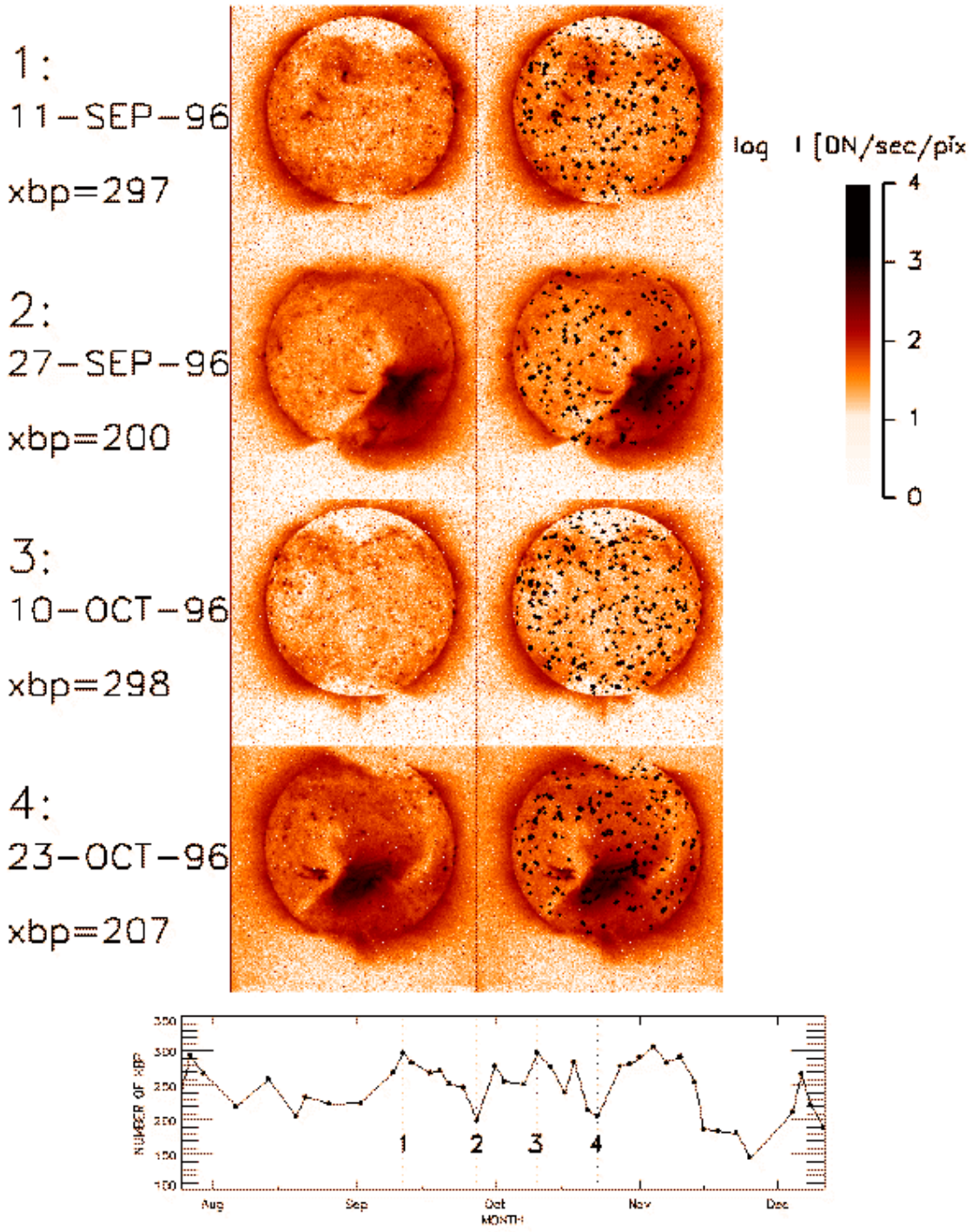

Figure 10.10: Bright points (observed number in soft X-rays, K. Nakakubo, NAOJ)

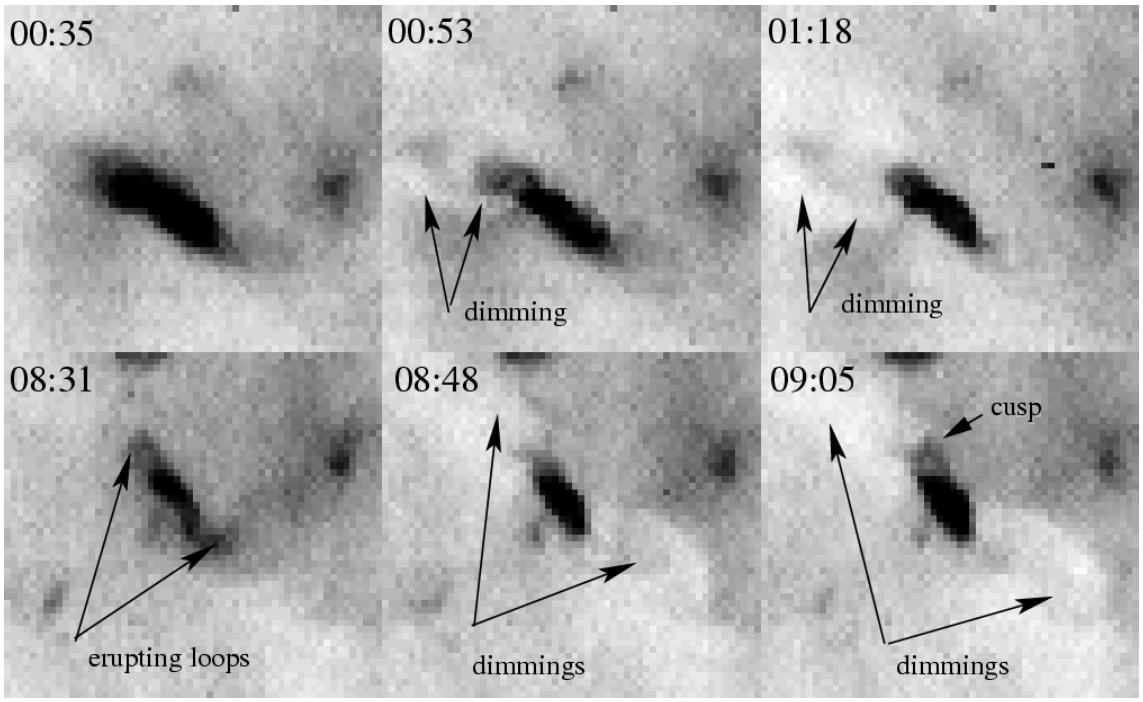

Figure 10.11: Bright points are sometimes 'mini active regions', that form S-shaped structures and erupt. This region showed even small-scale EIT dimmings. And surprisingly, the ejecta was identified near Earth, as coming from this region. Details can be found in the paper Mandrini et al., 2005: Interplanetary flux rope ejected from an X-ray bright point. The smallest magnetic cloud source-region ever observed.

10.4 Plumes

- Long, feathery jets with heights of about 30 $R_\odot$
- In unipolar regions (CH), but formed when bipolar flux emerges ('base' ~ bright point) $\Rightarrow$ small-scale reconnection driven by supergranular motion
- Dense: 3–5 $\times$ interplume densities
- SOHO CDS: temperature along plume structure ~ 1MK, base at ~ 2 MK
- Plume speeds 0–65 km/s, interplume speeds 105–150 km/s
- Oscillations of 20–25 min (slow magnetoacoustic waves?)
- Note that also fast solar wind in created in same CH regions

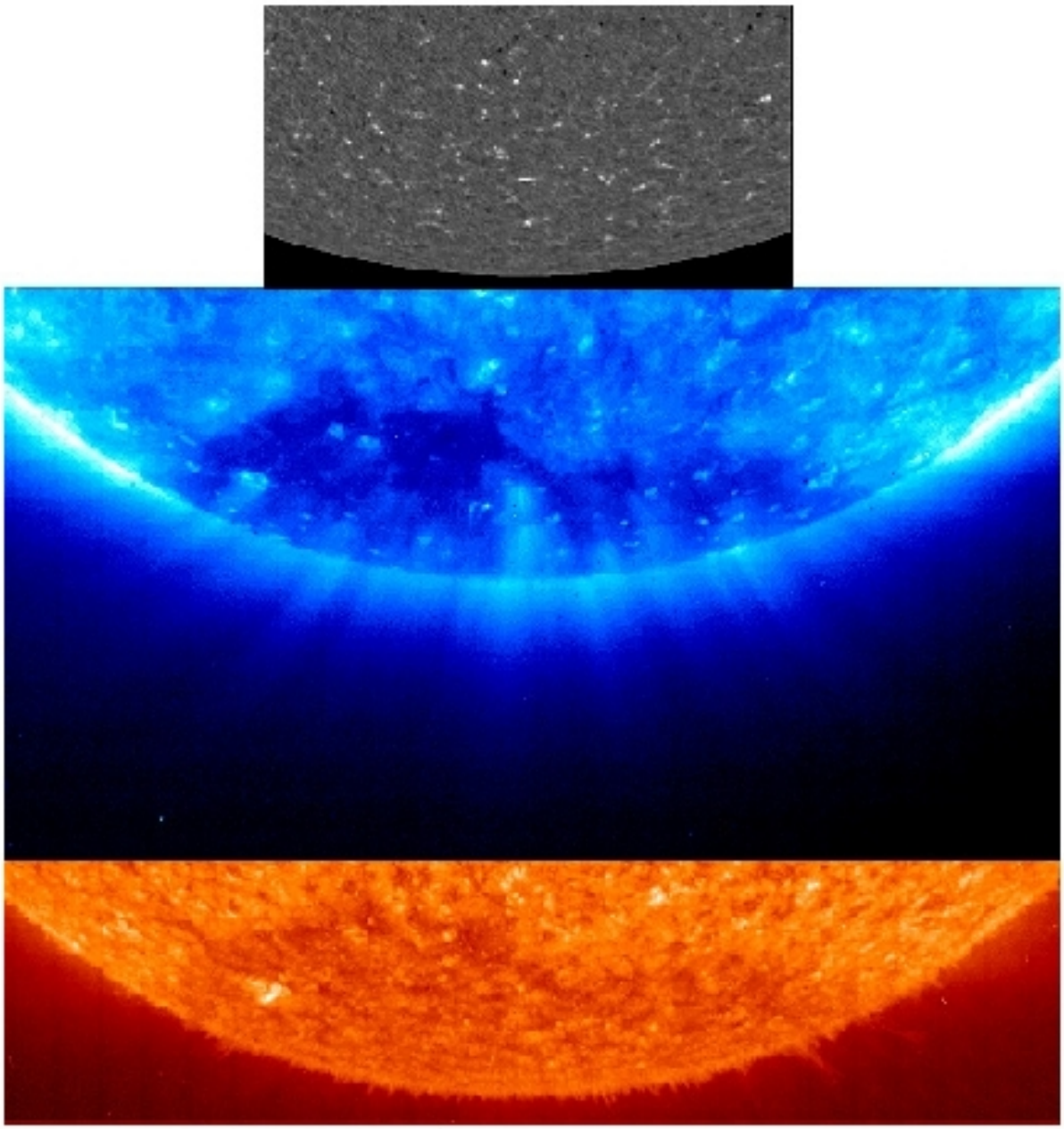

SOHO views of polar plumes
1996 March 7

Top to bottom:
MDI hi-res magnetogram
EIT Fe IX/X 171 Å image
EIT He II 304 Å image

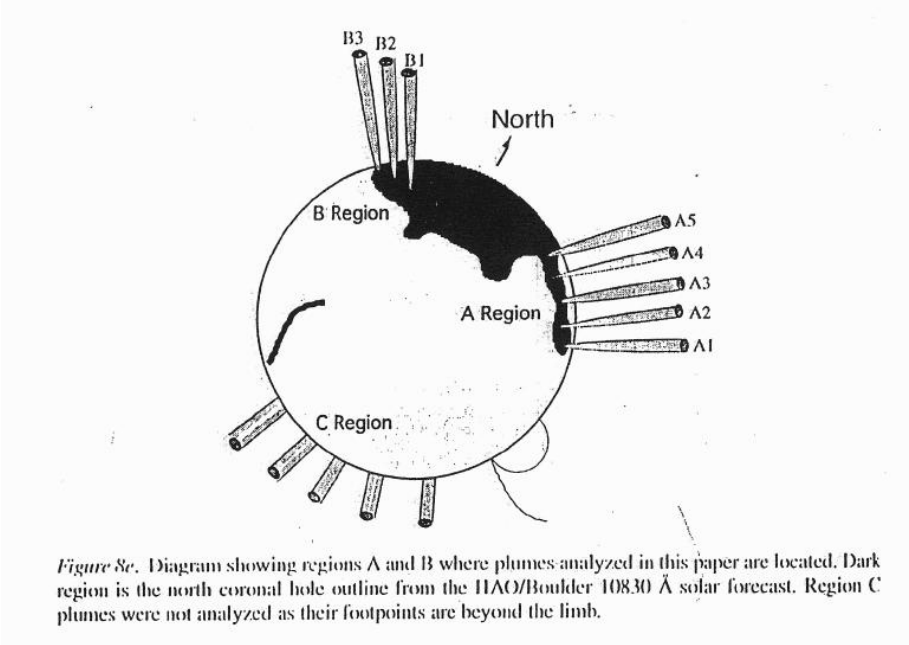

Figure 8c. Diagram showing regions A and B where plumes analyzed in this paper are located. Dark region is the north coronal hole outline from the HAO/Boulder 10830 Å solar forecast. Region C plumes were not analyzed as their footpoints are beyond the limb.

Figure 10.12: Allen & al. 1997, rocket experiments (still done, cheap and fast!)

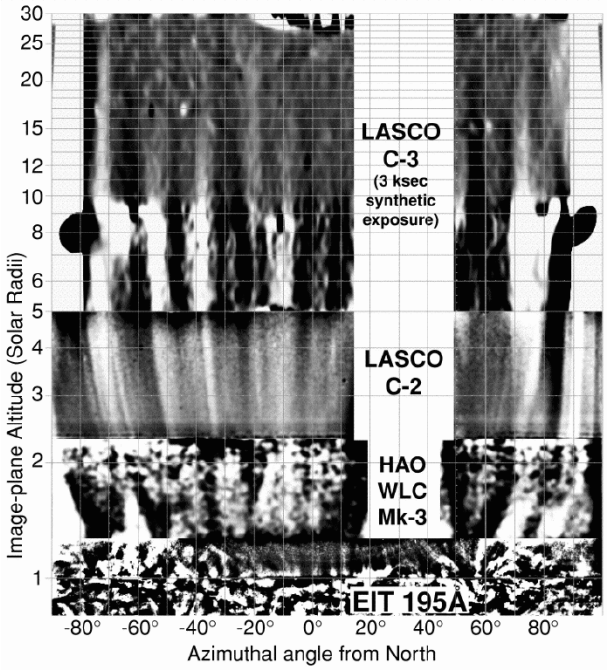

Figure 10.13: Polar plumes extending from the surface of the Sun out to 30 R_{sun} above the surface (in the image plane). Image is in conformal azimuthal coordinates. Vertical lines in image represent radial lines in normal space, and the radial direction is scaled logarithmically. Four instruments' data are presented. C-3, HAO K-Coronameter, and EIT images have been smoothed and detrended as described in text. C-2 image has been subjected only to radial filtering, to demonstrate by coalignment that the C-3 features are solar and not artificial. (DeForest et al, ApJ 546, 569-, 2001)

10.5 Spicules

- Fine, narrow jet-like structures near network boundaries, appear often in groups
- Heights 3000–9000 km (radio observations: ~7000 km)
- Speeds (Doppler) 10–30 km/s
- Lifetime ~ 10 min
- Unipolar magnetic field

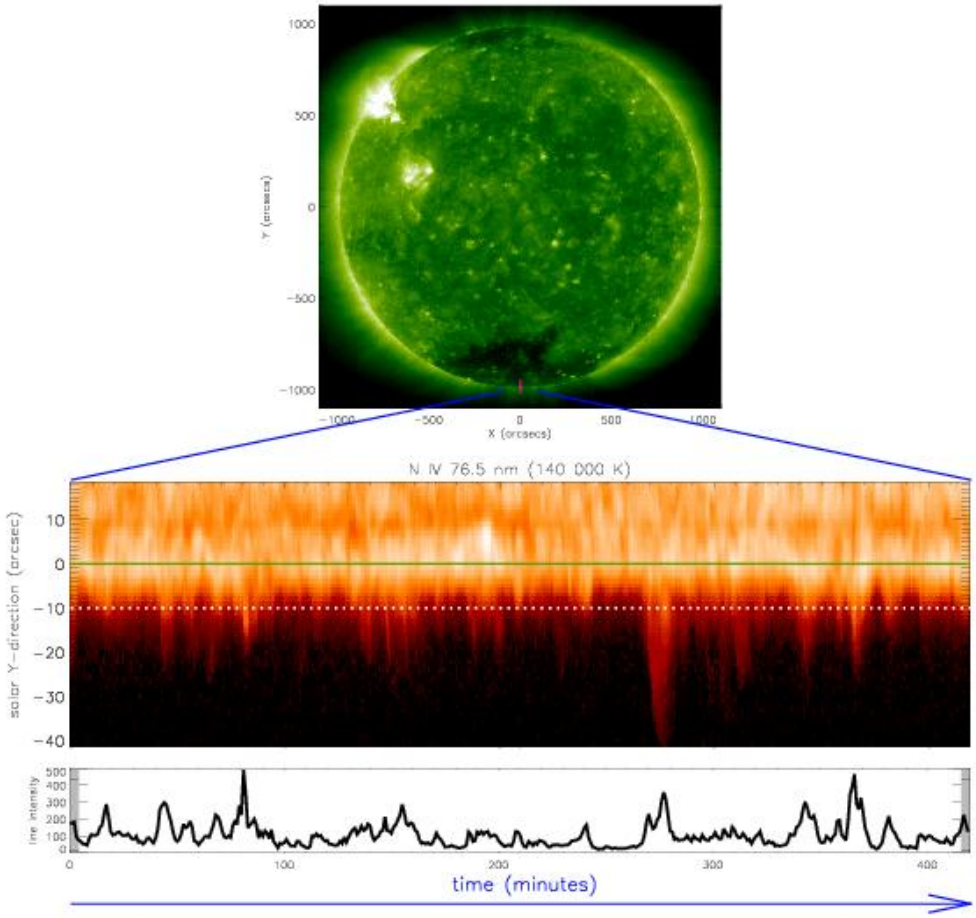

10.6 Photospheric network

- Granules (1000–2000 km)
- Mesogranules (5000–10 000 km)
- Supergranules (20 000–30 000 km)

Granules are created by cellular convection but larger structures are due to granular movements. At bright centers the flow is up and at dark edges the flow is downward.

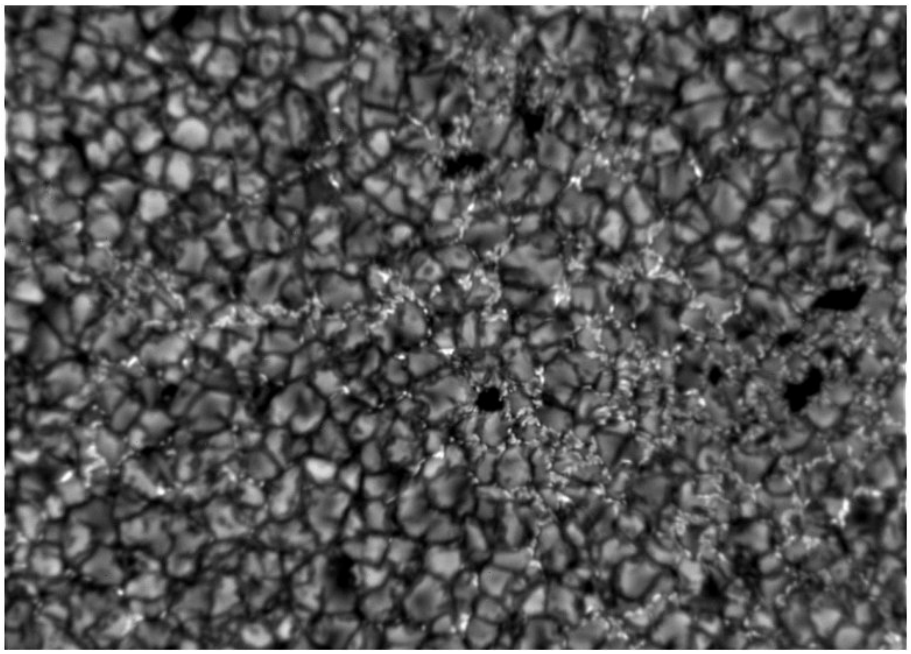

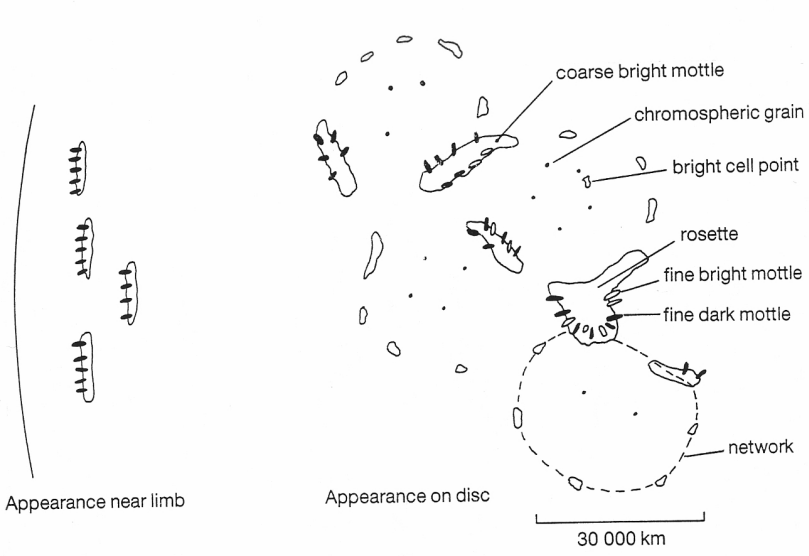

Fig. 4.8 Schematic diagram of quiet-sun chromospheric structures seen in Hα and Ca II H and K line images. The coarse bright mottles outline the chromospheric network, and fine dark and bright mottles emanate from the coarse mottles. At the intersection of two or three network cells, the fine mottles form a rosette pattern. Chromospheric grains are small dark features within network cells visible in the violet wing of the Hα line, while in Ca K bright cell points are small bright points that repeatedly brighten and fade. Near the limb the fine dark mottles seen in Hα point towards the limb.

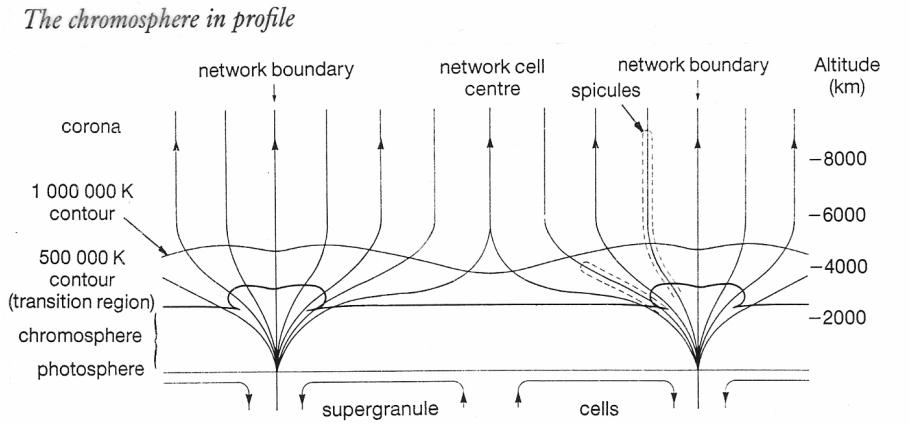

Fig. 4.2 Hypothetical section through chromosphere, showing the network structure and supergranules. Contours of temperature are shown for 500 000 K (taken to be the transition region) and for 1 000 000 K. The height scale on the right of the figure is only approximate. Spicules are represented by the dashed lines, the magnetic field lines by the arrowed lines: the field is swept horizontally towards the supergranule edges at low altitudes, but higher up the field lines spread out to form a canopy. (After Gabriel (1976))

Figure 10.14: (Plots from K.J.H. Phillips, Guide to the Sun, Cambridge Univ. Press)

10.7 Solar wind

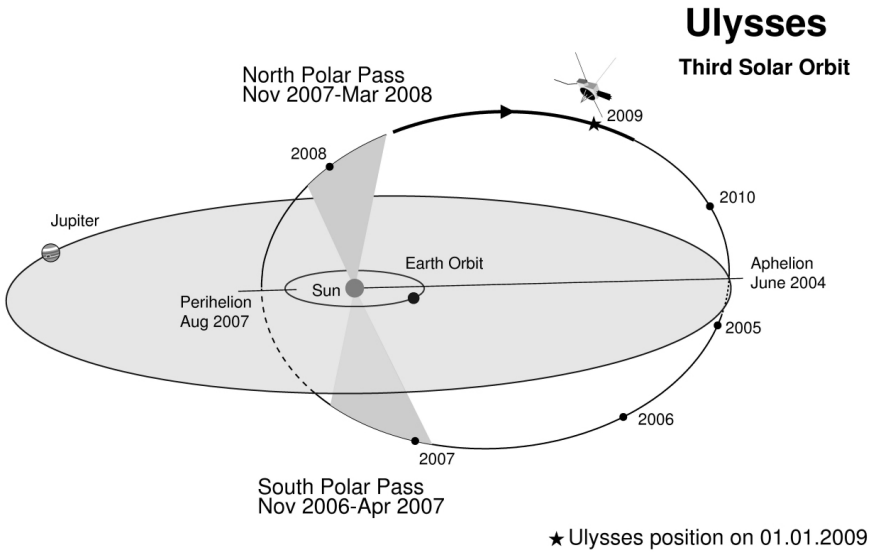

Figure 10.15: Ulysses spacecraft was launched in 1990. First south+north polar pass in 1994-95, second pass 2000-2001, third pass 2007-2008.

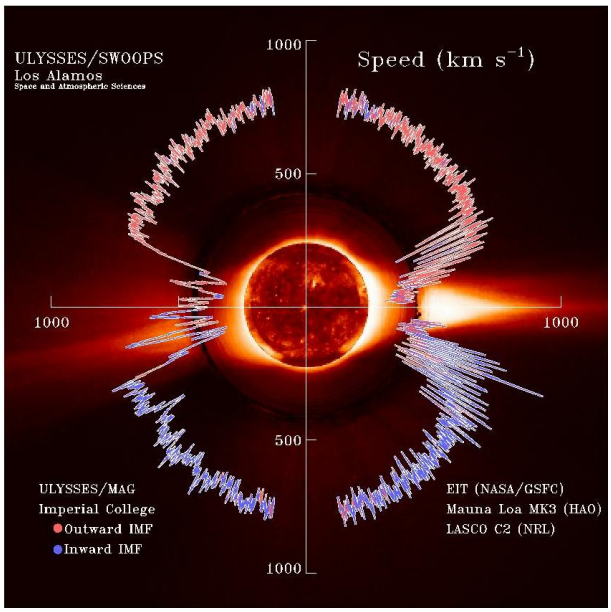

Figure 10.16: Solar wind speed (first solar pass)

Results from the first Ulysses bypass in 1994-95:
The solar wind is not uniform. Although it is always directed away from the Sun, it changes speed and carries with it magnetic clouds, interacting regions where high speed wind catches up with slow speed wind, and composition variations. The solar wind speed is high (800 km/s) over coronal holes and low (300 km/s) over streamers. These high and low speed streams interact with each other and alternately pass by the Earth as the Sun rotates. Many models of the solar magnetic field used prior to Ulysses assumed that the solar magnetic field was similar to that of a dipole; field lines near the solar equator were thought to form closed loops whereas field lines from the poles were dragged far into interplanetary space by the solar wind. For a dipole, the field strength over the poles is twice that at the equator. Ulysses found that the amount of outward magnetic flux in the solar wind did not vary greatly with latitude, indicating the importance of pressure forces near the sun for evenly distributing magnetic flux.

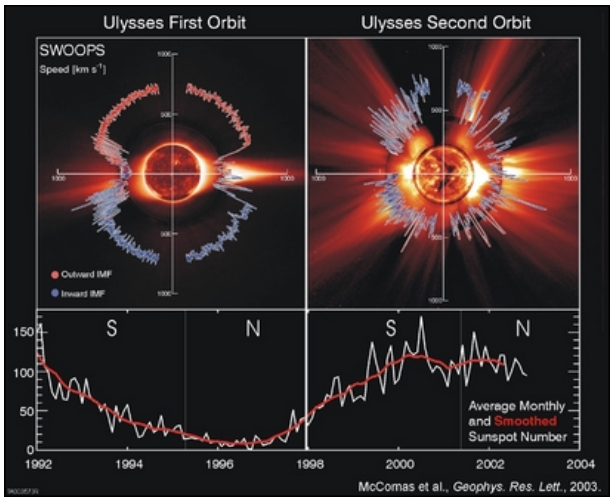

Figure 10.17: Solar wind speed during activity minimum (left, first pass) and during maximum activity (right, second pass).

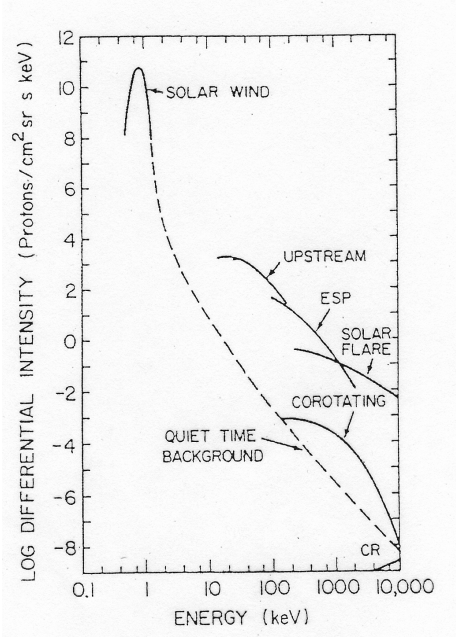

Figure 10.18: Energy spectra of different ion populations (Kallenrode, Space Physics). Particle loss due to solar wind is 1.3×10^{31} /s which is negligible when compared to the total solar mass.

10.8 Solar oscillations

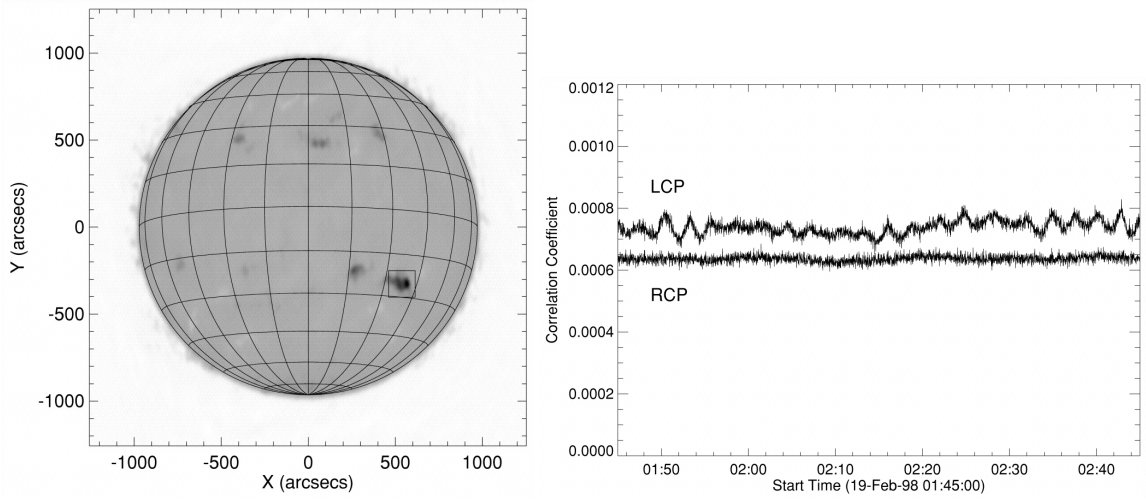

Figure 10.19: Full-disk intensity image of the Sun at 17 GHz (Nobeyama Radioheliograph). The active region is marked with a box. Correlation plot of 1 hour of observations for both RCP and LCP, showing that the emission was only left-hand polarized (Shibasaki, ApJ 550, 2001).

Gyrofrequency: $\nu_B \approx 2.8 \times 10^6 B$
If $B = 2000$ G, $\nu_B \approx 5.6$ GHz $\rightarrow 3^{rd}$ harmonic

The radio brightness temperature of an optically thin gyroresonance emission from the third harmonic layer is

$T_b = T\tau \propto T^3 N$

where T is the temperature and τ is the optical depth. The relative variation of the brightness temperature is then

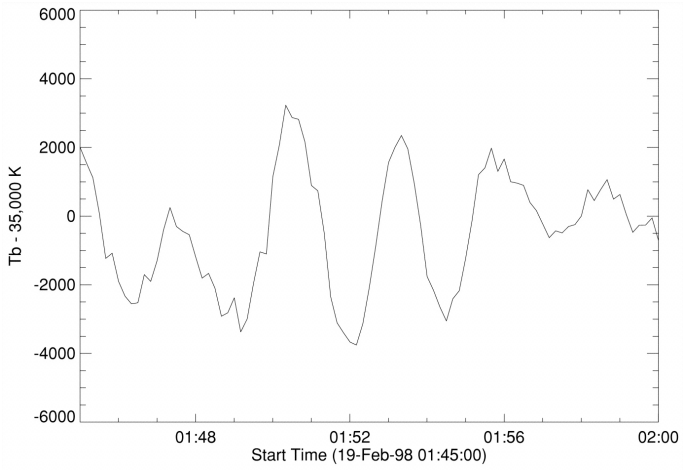

Figure 10.20: Time series of the peak brightness temperature during 15 minutes. The sunspot umbral oscillation was interpreted as density and temperature fluctuations due to upward-traveling acoustic waves through the third harmonic gyroresonance layer (2000 G).

$\frac{\delta T_b}{T} = \frac{3\delta T}{T} + \frac{\delta N}{N}$.

For an upward-travelling acoustic wave $\frac{\delta N}{N} = \frac{v}{c_S}$,

where c_S is the sound speed, v is the oscillation velocity amplitude, and N and δN are the density and its oscillation amplitude. From SUMER observations in EUV, the density oscillations $\frac{\delta N}{N}$ are approximated to be around 0.05 and the temperature oscillations $\frac{\delta T}{T} = (5/3 - 1)\frac{v}{c_S}$ around 0.03. Therefore,

$\frac{\delta T_b}{T} = \frac{3\delta T}{T} + \frac{\delta N}{N} = 3 \times 0.03 + 0.05 = 0.14$

As observed at 17 GHz, the oscillation intensity was $\frac{3000K}{25\,000K} = 0.12$,

and therefore the 3-minute oscillation period could be due to acoustic waves in sunspot umbra (Shibasaki, 2001).

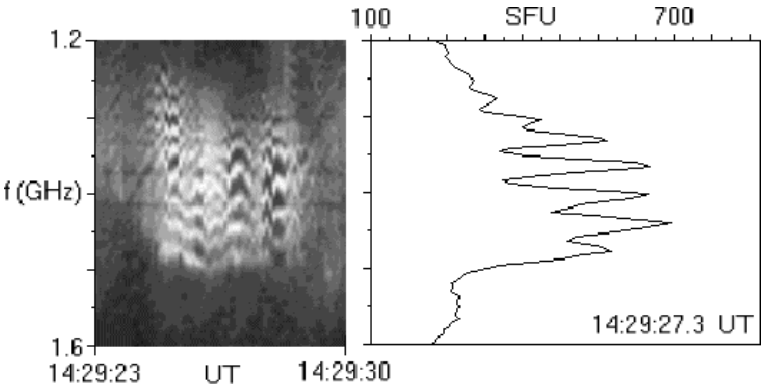

Figure 10.21: Example of an observed zebra-pattern, for which many alternative interpretations exist and this type of radio burst has already attracted attention for many years (Barta & Karlicky, A&A 450, 2006).

Solar radio pulsations show a large variety in their periods, bandwidths, amplitudes, temporal and spatial signatures. Most of them have been attributed to MHD oscillations in coronal loops, while alternative interpretations consider intrinsic oscillations of a nonlinear regime of kinetic plasma instabilities or modulation of the electron acceleration. In the umbral photosphere, oscillations with periods in the 5-minute range as well as in the 3-minute range occur. At chromospheric levels the intensity and velocity oscillations with periods of 150 – 200 s show larger amplitudes and are observed in the inner part of the umbra (Nindos & Aurass, Lecture Notes in Physics 725, 2007).

Microwave bursts often display quasi-periodic pulsations with periods from about 40 milli-sec in narrow-band bursts up to 20 sec in broad-band bursts (Nindos & Aurass). Causes of microwave flux pulsations with periods P ≈ 1 – 20 s are believed o be some kind of magnetic field variations that modulate the efficiency of gyrosynchrotron radiation or electron acceleration itself. Pulsations with longer periods can be associated with the slow magnetoacoustic mode which propagates almost along the magnetic field (Nakariakov & Stepanov, Lecture Notes in Physics 725, 2007).

10.9 Atmospheric models and coronal heating

One-dimensional atmospheric models were first built based on UV/EUV observations (e.g., the VAL model by Vernazza, Avrett, and Loeser, 1981; the FAL model by Fontenla, Avrett, and Loeser, 1993). It was soon discovered that these models predicted much higher radio brightness temperatures than what were observed at microwaves.

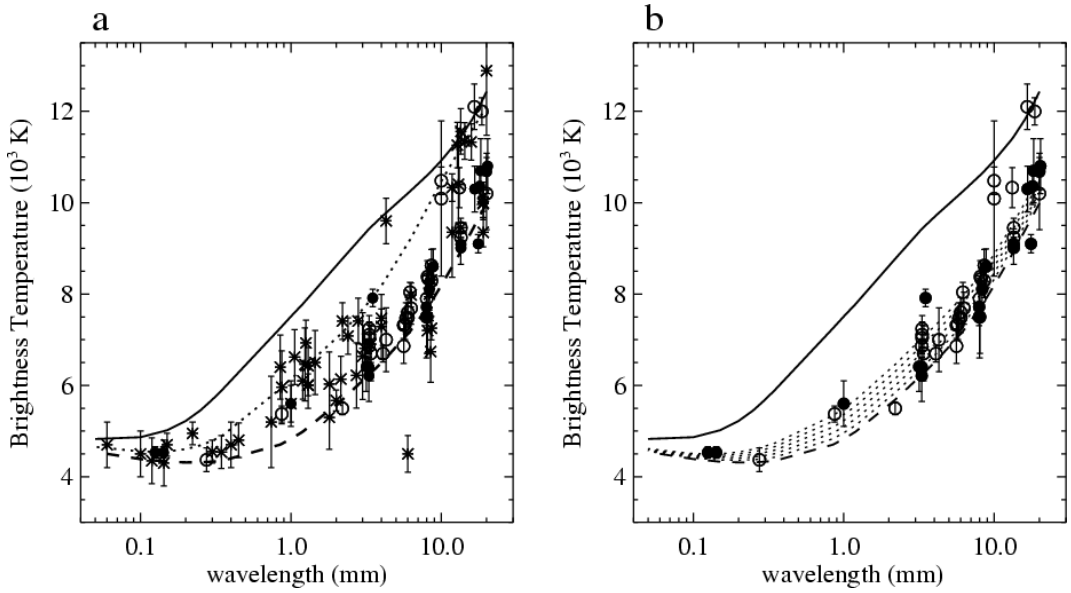

Figure 10.22: Observed brightness temperatures (circles and stars) and FAL models (dashed, dotted and solid curves), from Loukitcheva et al., A&A 419, 2004.

In 2003, Landi and Chiuderi Drago showed that a transition region model of the cell center, excluding any contribution from the magnetic network, can give an agreement with the observed radio brightness temperatures. The FAL models (a static atmosphere) and the dynamic simulations by Carlsson and Stein (1997 onwards) were compared with a large sample of radio observations in a study by Loukitcheva et al. (2004). The conclusion was that the dynamic picture of the solar internetwork chromosphere is consistent with the currently available millimeter and submillimeter brightness observations, although the chromospheric temperature rise is still absent in the simulations.

In other studies, a profound decrease in the computed temperatures have been obtained by assuming a tail of suprathermal electrons present in the solar atmosphere. Chiuderi and Chiuderi Drago (2004) modelled this with a two- component Maxwellian electron distribution and with a so-called kappa-function, and found both working.

Coronal heating

"There is no shortage of theoretical models that describe plasma-heating mechanisms that seem to be suitable for operating in the coronal environment (see discussion in Mandrini, Demoulin, & Klimchuk 2000), but the major dilemma is that either the theories are based on nonobservable parameters (e.g., currents, nonpotential magnetic energies, or coronal magnetic field) or the theoretical models have simply not been fitted to observed data. Another problem is that many theoretical models approximate a coronal loop with a straight cylindric tube, with a homogeneous density and magnetic field along the tube, while such an approximation is fully inadequate for large-scale loops observed in extreme ultraviolet (EUV), where the gravitational pressure scale height and heating scale height are much smaller than their half-length." (From Aschwanden, Astrophysical Journal, 560, 1035, 2001)

- DC-models: energy source is magnetic, release happens by e.g. reconnection (flares, nano-flares, pico-flares, etc.). For DC currents the characteristic time is larger than the Alfven transit time through the coronal magnetic structure.
- AC-models: energy source is convection or turbulence, transfer via MHD waves. AC coronal currents vary in a shorter time scale.

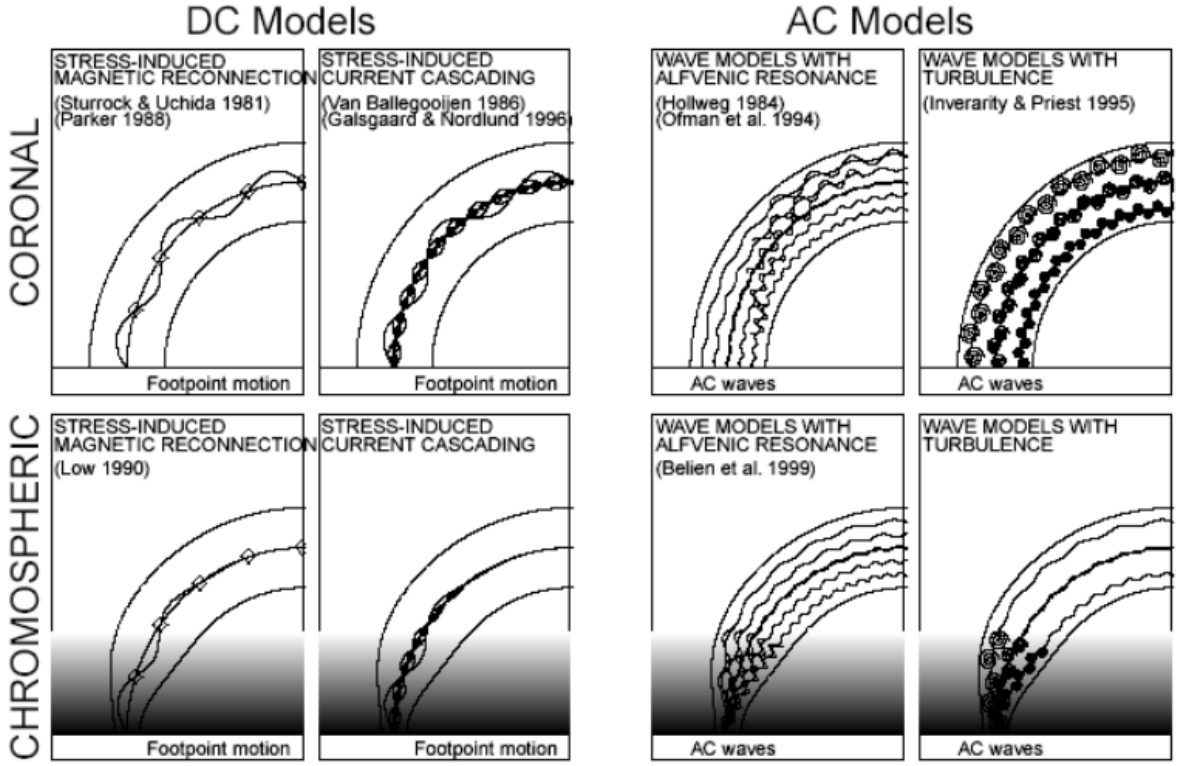

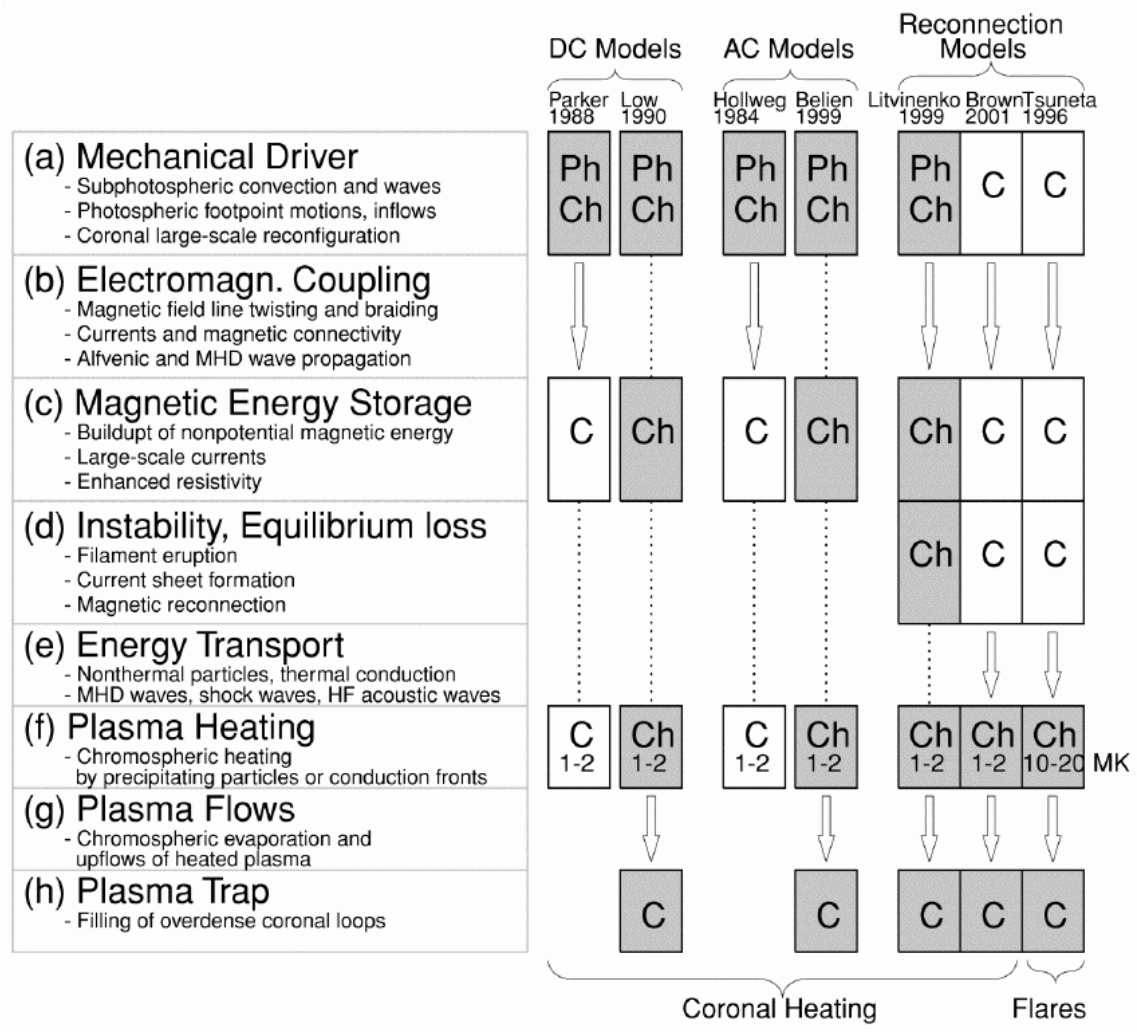

Figure 10.23: The eight main physical processes (ah) that occur in theoretical models of coronal heating are shown on the left side, and the corresponding flow charts of seven categories of theoretical models (with a reference to a typical representative listed at the top) are shown on the right side. Boxes mark the physical steps that are part of the models, arrows mark transport processes between different locations, and dotted lines mark cospatial locations. The boxes are colored in gray if the physical process takes place in a high-density region (photosphere, chromosphere, overdense coronal loops) and appear white for low-density regions (coronal background plasma). (Aschwanden ApJ 560, 1035-, 2001)

TABLE 1

CORONAL HEATING MODELS AND MATCHING OF OBSERVATIONAL CONSTRAINTS

Theoretical Model	Overdensity	Chromospheric Upflows	Heating Scale Height	References
Coronal DC Stressing				
Stress-induced reconnection				
Coronal	No	No	No	1, 2, 3, 4, 5, 6
Chromospheric	Yes	Yes	Yes	7
Stress-induced current cascade				
Coronal	No	No	No	8, 9, 10
Chromospheric	?	?	?	
Stress-induced turbulence				
Coronal	No	No	No	11, 12, 13, 14, 15, 16
Chromospheric	?	?	?	
Coronal AC Wave Models				
Alfvénic resonance				
Coronal	No	No	No	17, 18
Chromospheric	?	?	?	
Resonant absorption				
Coronal	No	No	No	19, 20, 21, 22, 23, 24, 25
Chromospheric	Yes	Yes	Yes	26
Phase mixing				
Coronal	No	No	No	27, 28, 29
Chromospheric	?	?	?	
Current layers				
Coronal	No	No	No	30
Chromospheric	?	?	?	
Turbulence				
Coronal	No	No	No	31
Chromospheric	?	?	?	
Magnetic Reconnection Models				
Dipolar				
Coronal	Yes	Yes	Yes	32
Chromospheric	Yes	Yes	Yes	33
Photospheric	Yes	Yes	Yes	34, 35, 36, 37, 38
Tripolar				
Coronal	Yes	Yes	Yes	
Chromospheric	Yes	Yes	Yes	39
Photospheric	Yes	Yes	Yes	
Quadrupolar				
Coronal	Yes	Yes	Yes	40
Chromospheric	Yes	Yes	Yes	
Photospheric	Yes	Yes	Yes	41

REFERENCES.—(1) Sturrock & Uchida 1981. (2) Berger 1991. (3) Parker 1988. (4) Berger 1993. (5) Galsgaard & Nordlund 1997. (6) Parker 1983. (7) Low 1990. (8) Van Ballegooijen 1986. (9) Hendrix et al. 1996. (10) Galsgaard & Nordlund 1996. (11) Einaudi et al. 1996. (12) Dmitruk & Gomez 1997. (13) Heyvaerts & Priest 1992. (14) Inverarity et al. 1995. (15) Inverarity & Priest 1995a. (16) Milano et al. 1997, 1999. (17) Hollweg 1984. (18) Litwin & Rosner 1998. (19) Ionson 1978, 1982, 1983. (20) Mok 1987. (21) Davila 1987. (22) Steinolfson & Davila 1993. (23) Ofman et al. 1994a, 1994b, 1995. (24) Halberstadt & Goedbloed 1995a, 1995b. (25) Ruderman et al. 1997. (26) Belien, Martens, & Keppens 1999. (27) Heyvaerts & Priest 1983. (28) De Moortel et al. 1999. (29) De Moortel, Hood, & Arber 2000. (30) Galsgaard & Nordlund 1996. (31) Inverarity & Priest 1995b. (32) Brown et al. 2000. (33) Litvinenko 1999. (34) Longcope & Kankelborg 1999. (35) Furusawa & Sakai 2000. (36) Sakai et al. 2000a, 2000b, 2001a, 2001b. (37) Tarbell et al. 1999. (38) Ryutova et al. 2001. (39) Chae et al. 1999. (40) Aly & Amari 1997. (41) Sturrock 1999.

Figure 10.24: Coronal Heating Models and Matching of Observational Constraints (Aschwanden, ApJ 560, 1035-, 2001)